Chapter 36

Meeting the Challenge of Monitoring Chlorophyll in the Ocean from Outer Space

André Morel
Laboratoire d'Océanographie de Villefranche, Université Pierre et Marie Curie, and CNRS, BP 8, 06238 Villefranche-sur-mer, France

Summary

Detecting and measuring, from space, the chlorophyll (Chl) content within the upper layer of the ocean, where the concentration is so low and the Chl-bearing phytoplanktonic cells are so small, can appear to be an impossible task. Further, a satellite-borne sensor directed towards the ocean captures the dominant atmospheric signal, due to light scattered by air molecules and aerosols, so that the marine signal must be extracted from this invasive background. Ocean color sensors, however, have been developed and now provide, on a daily basis, maps of the Chl distribution over the oceans of the world. This chapter explains how this challenge was faced and finally solved. These solutions involved the so-called 'bio-optical' properties of open ocean waters; namely, the existence in these waters of empirical relationships between the whole biogenic material, which governs the bulk optical properties, and a single component, the Chl content which can be detected and estimated from space by ocean color sensors. With newly developed sensors, it is now also possible to detect natural sun-stimulated Chl *a* fluorescence of phytoplankton which also provides a new promising approach to derive information about the physiological state of algal populations. The method of retrieving the marine signal and making the 'atmospheric correction' is briefly described. Paradoxically, this correction itself provides highly valuable information on the atmospheric aerosols, a crucial component of the radiative budget of our planet.

*Author for correspondence, email: morel@obs-vlfr.fr

Bernhard Grimm, Robert J. Porra, Wolfhart Rüdiger and Hugo Scheer (eds): Chlorophylls and Bacteriochlorophylls: Biochemistry, Biophysics, Functions and Applications, pp. 521–534.

I. Introduction

The determination of the chlorophyll (Chl) concentration within water bodies from space-based observation platforms could be deemed, a priori, as an impossibility for at least two reasons: Firstly, our planet as seen from space, is essentially blue as a result of its gaseous atmosphere that efficiently scatters back the incident solar radiation; consequently, information captured within the visible spectral range by any space-borne sensor directed at the ocean is largely dominated (> 90%) by this atmospheric signal. Secondly, the Chl concentration within the open ocean is rather low (approx. 0.20 mg Chl per m^3 of sea water, on average), making its detection a considerable challenge. Nevertheless, this challenge was accepted, and 'ocean color' measurements (through remote spectroscopy) were carried out from an airplane (Clarke and Ewing, 1974). The first ocean color satellite sensor, CZCS (Coastal Zone Color Scanner) was launched in 1978 and demonstrated the feasibility of such a technique. Currently, 'chlorophyll-maps' of the entire ocean are produced every day, thanks to new sensors such as SeaWiFS (Sea-viewing Wide Field-of-view Sensor), MODIS (Moderate Resolution Imaging Spectrometer), MERIS (Medium Resolution Imaging Spectrometer), and others. As Chls are the pigments ultimately responsible for photosynthesis and primary production, the determination of the concentration of the predominant Chl, Chl *a,* remains an essential research tool in biological oceanography, in marine ecology and in the study of bio-geochemical cycles, particularly of the carbon cycle.

From ancient times, mariners and fishermen have found significance in the changing color of the sea. From coastal turbid zones to open sea areas, the color evolves in a distinctive way. Also, in the open sea, the color may change from a dark deep green to intense blue as the observer moves from eutrophic waters with a high phytoplankton concentration to oligotrophic limpid waters with an extremely low phytoplankton content. This color shift has been an indication of food abundance for experienced fishermen and is the rationale for the detection and quantification of algal concentrations.

The physical translation of the human perception of color is the spectral reflectance, $R(\lambda)$, which is defined at each wavelength (λ) as the ratio of upwelling irradiance to downwelling irradiance just beneath the interface (denoted 0^-), so that the reflection of the skylight at the interface is ignored

$$R(\lambda) = E_u(0^-, \lambda) / E_d(0^-, \lambda) \quad (1)$$

The downward flux, $E_d(0^-, \lambda)$, originates from the (direct) solar radiation and the (diffuse) sky radiation. Its spectral composition depends on the zenith-sun angle and on the atmospheric properties (aerosol load and composition). The magnitude of the upward flux within the water body, $E_u(0^-, \lambda)$, is intuitively related to the two antagonistic processes of backscattering, which allows the downward photons to travel backwards, and of absorption, which annihilates photons and so cancels their chance of being backscattered. This heuristic approach translates into an expression of the following form:

$$R(\lambda) = f\,[b_b(\lambda)/a(\lambda)] \quad (2)$$

It involves the ratio of the backscattering-(b_b)- and the absorption-(a)-coefficients of the water body: these coefficients represent the probability of backscattering and absorption per unit length along the path of a beam, respectively (with the units m^{-1}). A more accurate approach uses the radiative transfer equation (RTE) which describes the radiance field within a scattering-absorbing medium, and relates radiation propagation to the inherent optical properties of the medium, namely, the absorption and scattering coefficients and the volume scattering function. Sophisticated computations using the RTE confirm, as expected, that the first determinant of $R(\lambda)$ is the ratio $[b_b(\lambda)/a(\lambda)]$.

These accurate computations also allow the assessment of the dimensionless factor, f, and the prediction of its variations which depends on wavelength (λ) and varies between approx. 0.3 and 0.5 dependent mainly on the solar angle. The backscattering coefficient includes the effects of both water molecules and suspended particles within the water body, while the absorption coefficient results from the water itself and from all the dissolved and particulate absorbing substances it contains. Herein lies the basis for remote

Abbreviations: Chl(s) – chlorophyll(s); [Chl] – chlorophyll *a* concentration; CZCS – Coastal Zone Color Scanner (NASA, launched 1978, stopped 1986); MERIS – Medium Resolution Imaging Spectrometer (ESA, launched 2002, in-flight); MODIS – Moderate Resolution Imaging Spectrometer (NASA, launched 2000, in-flight); NPP – net primary production; PAR – photosynthetically available radiation; RTE – radiative transfer equation; SeaWiFS – Sea-viewing Wide Field-of-view Sensor (NASA, launched 1997, in-flight); SST – sea surface temperature

sensing. Indeed, R(λ) will, to a first approximation, reflect in an inverse manner the absorption spectrum and would do so exactly if the backscattering (b_b) spectrum was perfectly flat. As the Chl pigments of the phytoplanktonic algae are extremely absorbing, they directly influence the shape of both the absorption and reflectance spectra.

Because of refraction and internal reflection, only about one half of the upward radiant flux (E_u) is able to emerge from the interface, and then to form the so-called 'water-leaving radiance' field. These exiting radiances, which carry information about the water content, propagate in all upward directions. They are partly attenuated (i.e., absorbed and scattered out) along their path through the atmosphere before reaching the orbiting sensor, whereas intense radiances, created by (multiple) scattering within the atmosphere, are added to the initial signal (see Fig. 1). The 'marine signal' is, therefore, 'nearly drowned' within a predominantly atmospheric signal.

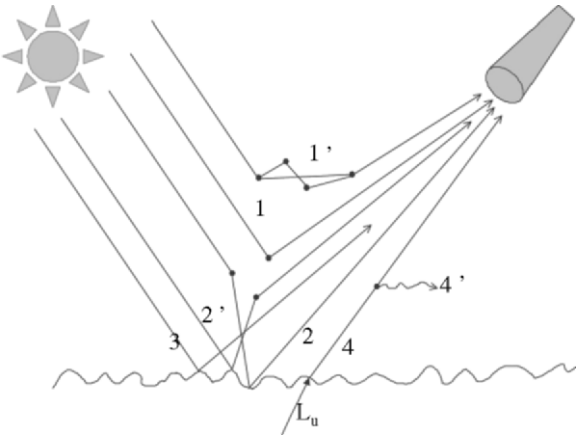

Fig. 1. Schematic representation of the various components forming the signal received by a satellite borne sensor directed at the ocean (wavy interface). Note that the sensor and the sun are generally not in the same vertical plane. The first component corresponds to solar photons scattered by atmosphere (i.e., by molecules or aerosols) toward the sensor; the path (1) describes a single scattering event, and (1′) double (or multiple) scattering events. Photons can be scattered and then reflected by the surface, or reflected and then scattered toward the sensor (paths 2 and 2′). The path (3) represents photons directly reflected back toward the sensor from the interface; if the sensor and the sun are in the same vertical plane and in symmetrical positions with respect to the zenith, the sensor aims at the specular image of the sun ('sun glint'); some sensors avoid this viewing angle (due to a tilt capability). Because of the presence of capillary waves, the sun glint is often much wider than the specular image. Finally, the in-water upward radiance L_u is the component which carries information: it propagates through the interface and forms the water-leaving radiance L_W (4); this radiance is partly attenuated (i.e., absorbed and scattered) by the atmosphere (4′), so that the radiance reaching the sensor is $t^* L_W$, where t^* represents the diffuse transmittance of the atmosphere (which depends on the aerosol load and ozone content).

II. Absorbing Substances in the Marine Environment

Two questions now arise. Are phytoplankters the only absorbers in the marine environment? Is chlorophyll the predominant absorbing pigment in phytoplankton? Both answers which, a priori, are 'no,' deserve some comments, since the determination of the chlorophyll concentration is the main goal.

In coastal areas, affected by river outflows, diversely colored sediments (inorganic and organic) are often abundant, and affect both the absorption and the backscattering processes. Absorbing dissolved substances, consisting of humic and fulvic acids, collectively called *'gelbstoff'* or yellow substance, are also brought to the sea by land drainage. These optically significant components generally vary independently of each other, and are independent of phytoplankton abundance. Such complex waters, categorized as 'Case 2 waters' (Morel and Prieur, 1977), are difficult to interpret, and the extraction of any chlorophyll 'signal,' interwoven with many others, remains difficult. In the open ocean, far from terrestrial influences, phytoplankton, and their co-existing retinue (virus, bacteria, other heterotrophs, as well as debris and dissolved organic substances) are recognized as the principal agents responsible for variations in optical properties (Morel and Prieur, 1977). In these so-called 'Case 1 waters,' which represent about 97% of the global oceans, the Chl concentration may span about three orders of magnitude (approx. 0.02 to 20 mg m^{-3}). The optical behavior of Case 1 waters is simpler and better understood than Case 2 waters, and thus their absorbing and scattering properties are more predictable as a function of the phytoplankton content. Below, emphasis will be put on these Case 1 waters; however, the specific problems raised by Case 2 waters have been examined in detail in a recent review (IOCCG, 2000).

In oceanic Case 1 waters, the absorption coefficient, a(λ), can be written as the sum:

$$a(\lambda) = a_w(\lambda) + a_{cdom}(\lambda) + a_p(\lambda) \quad (3)$$

where the subscripts w, cdom, and p represent water,

colored dissolved material, and particulate matter, respectively; this particulate matter consists of phytoplankton (subscript φ) and non-algal particles (subscript nap), thus, $a_p(\lambda) = a_\varphi(\lambda) + a_{nap}(\lambda)$.

The colored dissolved material is similar to the *gelbstoff* already mentioned, except that it is locally formed by excretion and/or decay of algal material. The non-algal particles essentially include debris and heterotrophic bacteria. Both $a_{cdom}(\lambda)$ and $a_{nap}(\lambda)$ exhibit a featureless spectrum characterized by an exponential increase towards the shorter wavelengths.

As an obvious consequence of Eq. 3, chlorophyll is not the only absorber. Even when considering the phytoplankton term, $a_\varphi(\lambda)$, a variety of absorbing accessory pigments, both photosynthetic and photoprotectant, are present in algal cells along with Chl *a*, or its derivative, [8-vinyl]-Chl *a* which has recently been found to be a major component in oceanic algae (Chapter 4, Kobayashi et al.). The pigment composition depends on species, and for a given species, often varies with such environmental conditions as light, depth and nutrients. In general, natural populations are mixtures of many species, although a single phytoplankton species may predominate in temporary 'bloom' conditions. These organisms encompass a wide size range, from >20 μm (diatoms, dinoflagellates) to ~ 0.5 μm (for abundant prokaryotes such as *Prochlorococcus*). The size of the individual cells has a strong influence on the effective absorption coefficient for a given internal pigment concentration. This physical phenomenon, termed the 'package effect' (Duysens, 1956), affects the relationship between the pigment content and the absorption coefficient (Morel and Bricaud, 1981). This effect, along with varying pigment compositions, explains that the 'Chl-specific' absorption spectra of phytoplankton (cultivated or natural) are far from being immutable (Fig. 2 a,b).

Nevertheless, all these spectra exhibit a sharp red peak near 675 nm, essentially due to Chl *a*, and a

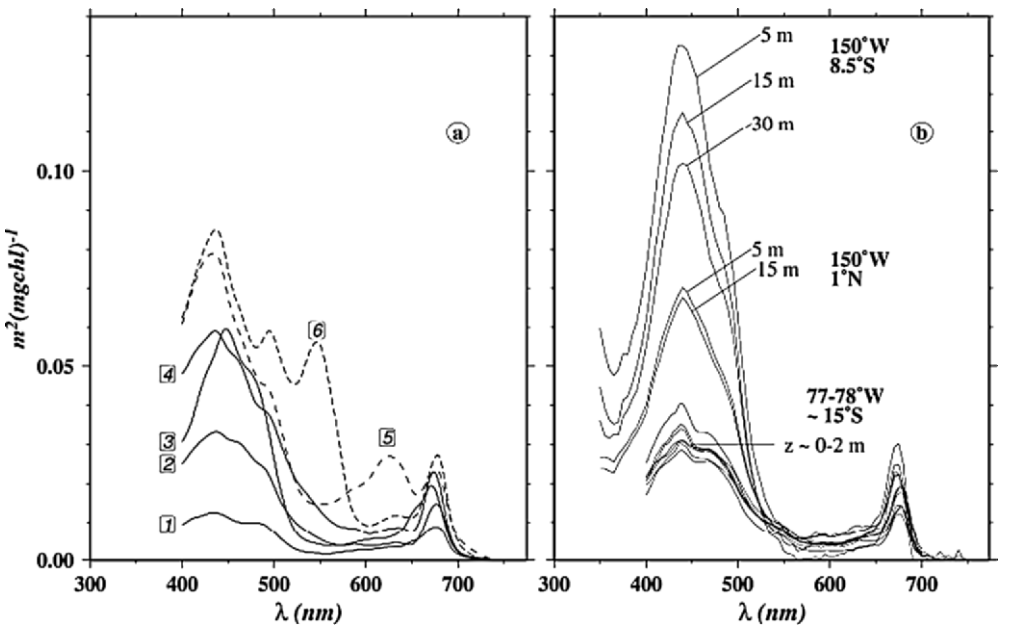

Fig. 2. (a) Examples of chlorophyll-specific absorption coefficients, aφ (λ), determined directly on suspensions of various phytoplankters grown in culture at moderate irradiance (see in Stramski et al. 2001); namely, 1 *Dunaliella bioculata*, 2 *Prymnesium parvum*, 3 *Chaetoceros curvisetum*, 4 *Prochlorococcus* sp. , 5 *Anacystis marina*, 6 *Synechococcus* sp. For the cyanobacteria (labeled 5 and 6), the presence of phycocyanin, phycoerythrin, and phycourobilin is indicated by the peaks at 630, 545, and 490 nm, respectively. Such prominent peaks, typical of monospecific cultures, are considerably smoothed in natural algal assemblages. (b) Examples of chlorophyll–specific absorption spectra for natural populations (determined using the in vitro filter technique) in three differing trophic regimes (all in the Pacific Ocean), namely: oligotophic situation in the southern gyre (8.5°S), mesotrophic conditions near the Equator (1°N), and eutrophic conditions within the Peruvian upwelling area: [Chl] are 0.13, 0.30, and 3 mg m^{-3}, respectively (see also Fig. 7); the sampling depths (m) are also indicated. Note that, in contrast to the data for pure cultures (panel a) , these spectra include the effect of accompanying non-algal particles and thus correspond to $a_p(\lambda)$ in Eq. 3.

broad absorption band in the blue 400–500 nm domain which peaks around 440 or 448 nm for Chl *a* or [8-vinyl]-Chl –*a*, respectively: these spectra are variously shaped as a result of changing pigment composition. The actual contribution of Chl *a* to the global absorption within this blue band largely varies between about 30 and 70%, and Chl *b*,*c* together with carotenoids, are responsible for the additional absorption. In the green 540–600 nm region of the spectrum, algal absorption is at its minimum, except when phycobilins are present, as in cyanobacteria. A second observation is the wide (~ten-fold) variation of the blue absorption per unit of Chl *a*, not only for an individual species (Fig. 2a), but equally for naturally-occurring mixed populations (Fig. 2b). In summary, the influence of other pigments, such as Chl *b,c* and various carotenoids, together with a more or less pronounced package effect, are responsible for the observed variability in total algal absorption, in so far as absorption has been normalized with respect to Chl *a* content.

These typical algal absorption spectra exhibit intense absorption in the blue region when compared with that of pure seawater (Fig. 4b), which, in contrast, shows extreme transparency in the blue and high absorption in the red. Therefore, even a trace of phytoplankton enhances the blue absorption and thus depresses blue reflectance. The red absorption peak which is essentially attributable to Chl *a*, however, remains indiscernible in the background water absorption, even in the presence of large algal concentrations. The green region of the spectrum, where algal absorption is minimal, is less sensitive to the presence of phytoplankton. Since the blue absorption cannot be attributed to Chl *a* alone, as already discussed, the capability of ocean color sensors for providing synoptic views of the Chl *a* distribution, based on the blue absorption, is necessarily limited.

Historically, only Chl *a* was routinely determined at sea, using either spectrophotometry or fluorometry. Consequently, its concentration, denoted [Chl], was the single index available when studying the so-called 'bio-optical' properties of water bodies (i.e., absorption, scattering, backscattering, diffuse attenuation and reflectance). These studies have resulted in empirical relationships between the bulk optical properties, which account for all pigments and substances, and the chlorophyll concentration alone. These relationships, established for Case 1 waters, remain fundamental for the algorithms which are presently applied to ocean color data to calculate [Chl]. This situation will change with the widening use of high performance liquid chromatography which allows many pigments to be quantified (see Chapter 8, Garrido and Zapata).

III. Bio-optical Relationships in Oceanic Waters and Chlorophyll Algorithms

The simplest approach consists of relating [Chl] directly to $R(\lambda)$, when both have been simultaneously measured at sea (Morel and Prieur, 1977; Smith and Baker, 1978). If statistically significant relationships exist between the two quantities, they can be used as algorithms. As the presence of algae strongly depresses the reflectance in the blue region of the spectrum and does not significantly affect the green reflectance, the strategy was to form a ratio of reflectances at two wavelengths, $R(\lambda_1)/R(\lambda_2)$, where λ_1 and λ_2 are located in the blue and green regions of the spectrum, respectively (see Table 1). Such ratios systematically decrease when [Chl] increases (Fig. 3). A polynomial fit to such data, within the log-log space, can be used to retrieve [Chl] from the reflectance ratios in Case 1 waters. Such algorithms (O'Reilly et al., 1998) are called 'purely empirical'.

'Semi-analytical' algorithms are derived from the use of Eq. 2 and on the additivity principle which applies to the backscattering and absorption coefficients. Various parameterizations of both these coefficients as a function of [Chl] have been proposed, leading to slightly different reflectance models (Lee et al., 1994). The total absorption coefficient (see Eq. 3), involves $a_{CDOM}(\lambda)$ and $a_p(\lambda)$. These partial coefficients can be related to [Chl] through empirical relationships (valid for Case 1) by measuring separately the absorption by both dissolved and particulate matter. For instance (Fig. 4a), the absorption coefficient a_p (at 440 nm) has been found to increase along with [Chl], but in a non-linear manner (Bricaud et al., 1998), as described by Eq. (4):

$$a_p(440) = 0.0520\ [\text{Chl}]^{0.635} \qquad (4)$$

On average, the partition of a_p between the non-algal and the algal compartment is about 30%–70%, respectively (see Fig. 4a). Expressions similar to Eq. 4 have been obtained for all wavelengths through regression analyses. In these expressions, the coefficient and the exponent are wavelength (λ) dependent so that the shape of the absorption spectrum changes

Table 1. Relevant information and main characteristics of several Ocean Color sensors (detailed information in IOCCG, 1998). These sensors are polar orbiting and sun synchronous with an equatorial crossing time between 10 am and noon (local time). Their altitude is about 700–800 km. With about 14 orbits per day, a total coverage of the earth is obtained within 3 days at the Equator, 2 days at mid latitude and in one day at high latitude. The spectral channels dedicated to ocean color and atmospheric correction (listed below) are 10 to 20 nm wide, except the narrower channels devoted to fluorescence detection. Note that the fluorescence channels are not centered on the maximum of the fluorescence peak (at 683 nm), because of the interference with an atmospheric absorption band due to O_2 (687–693 nm).

CZCS	SeaWiFS	MODIS	MERIS	Information retrieved
Channels (central wavelength [nm])				
	412	412.5	412.5	Gelbstoff detection
443	443	443	442.5	Phytoplankton absorption maximum
	490	488	490	Phytoplankton absorption
520	510	531	510	Hinge point for reflectance
550	555	551	560	Phytoplankton absorption minimum
670	670			Sediment detection
		667	665	Baseline for fluorescence detection
		678	681.25	Chlorophyll-a fluorescence detection
			709	Baseline for fluorescence detection
	765	748	779	Aerosol detection/quantification
	865	869.5	870	Aerosol detection/quantification
Swath (Km)				
1566	1800 (1200)*	2330	1150	*GAC mode (Global Area Coverage)
Resolution at nadir (Km),				in LAC (Local Area Coverage) mode
0.825	1.1 (4.4)*	1.0	0.3 (1.2)*	*for GAC mode

slightly and progressively with the concentration. Examples of spectra resulting from the sum $[a_w(\lambda) + a_p(\lambda)]$ are displayed in Fig. 4b. Several reasons for the natural non-linear, albeit regular, trend (expressed by Eq. 4) have already been identified. Among them, the changing mean cell size of unicellular algae is likely to be the most important (Bricaud et al., 2004). In oligotrophic waters ([Chl] <0.1 mg•m^{-3}), phytoplankton are dominated by minute species with a reduced package effect (i.e., maximal absorption per unit of Chl); in contrast, large species, with a more pronounced package effect (i.e., lesser absorption per unit Chl), prevail in eutrophic waters ([Chl] >1 mg•m^{-3}). In oligotrophic tropical waters, carotenoid-to-Chl ratios are often higher in the upper layer, where photoprotecting carotenoids are present in larger quantities in algal cells. Anyway, the carotenoids (both photoprotectant and light-harvesting pigments) contribute to the enhancement of algal absorption in the blue-green part of the spectrum. In summary, when [Chl] increases in the natural environment there is a progressive, rather regular, lowering of a_p*, the Chl-specific absorption coefficient (i.e., per unit of Chl, and expressed as m^2•mg^{-1}). With such a propitiously regular change of a_p* values, retrieval of [Chl] is possible: with random changes, retrieval would have been problematic.

The backscattering coefficient (Eq. 2) is the sum of the coefficients for pure water and for suspended particles, b_{bw} and b_{bp}, respectively. The contribution of water molecules is large; it is actually dominant for most oceanic waters (Fig. 5). The b_{bw} coefficient, varying as $\lambda^{-4.3}$ (Rayleigh-type scattering), thus strongly increases towards the shorter wavelengths, and accounts for the deep-blue color of clear oligotrophic waters. The parameterization of b_{bp} is generally performed in two steps. Firstly, based on regression analyses of field measurements in Case 1 waters (Gordon and Morel, 1983), the scattering coefficient, b_p, can be empirically related to [Chl]; again, non-linear relationships emerge as expressed in Eq. 5 (see Loisel and Morel, 1998):

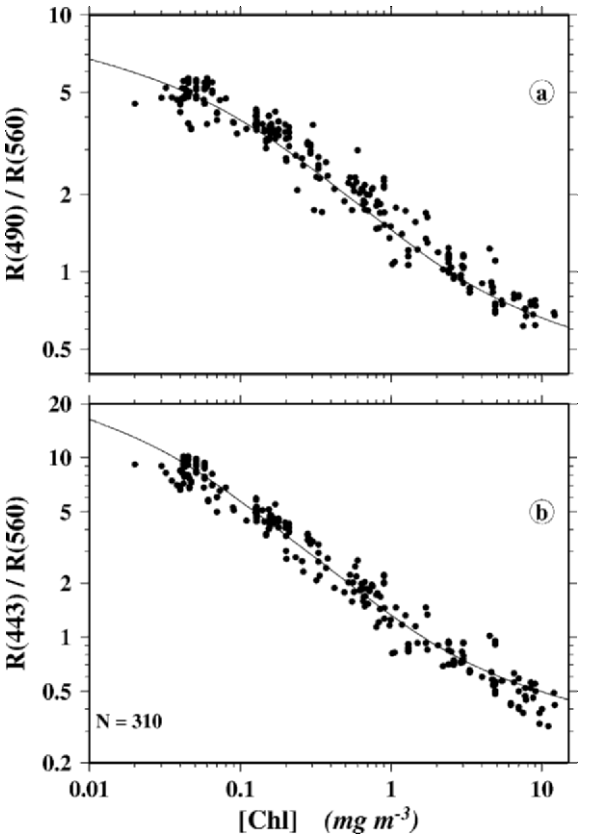

Fig. 3. Ratios of reflectance at two wavelengths (490–560 nm in a, and 443–560 nm in b), forming 'blue-to-green' ratios as a function of the chlorophyll concentration (log-scales). The curves have been produced via a predictive semi-analytical model (based on absorption and backscattering; see text and also Fig. 6a), whereas the dots are independently derived from paired measurements (N= 310) of reflectance and chlorophyll made in various parts of the world's oceans. Actually, the semi-analytical model and a purely empirical model (i.e., the best polynomial fit for the data) are very similar, as it can be guessed from these graphs.

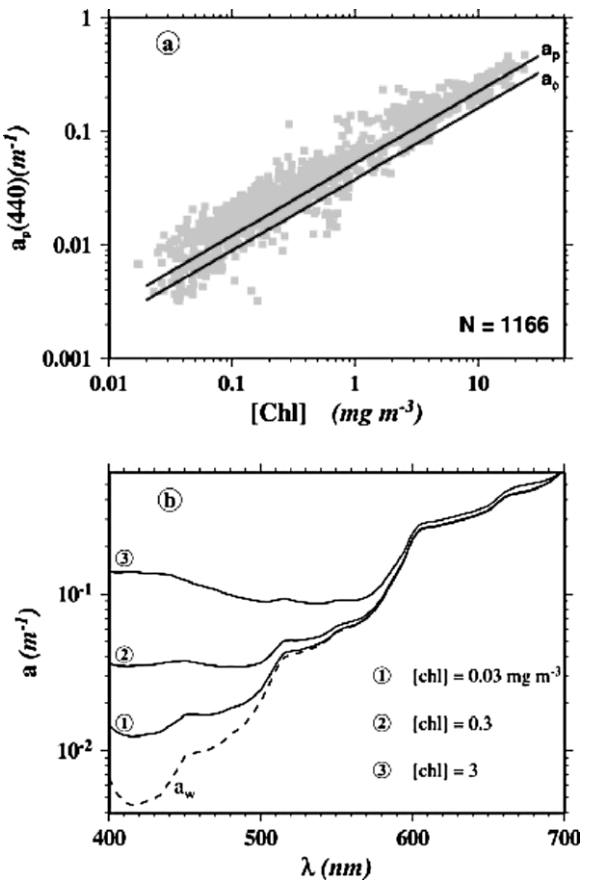

Fig. 4. (a) Simultaneous field measurements of the absorption coefficient at 440 nm by total particulate matter, a_p, (filter technique, Yentsch, 1962), and of the chlorophyll concentration (1166 couples of data, plotted with log-scales, as closed squares). The empirical straight line, denoted a_p, corresponds to Eq. 4. By extracting the pigments from the particles retained onto the filter (Kishino et al., 1985), and measuring the residual absorption, the non-algal and algal contributions to particle absorption can be separately assessed (Eq. 3). The line, denoted a_φ, is also obtained through regression analysis applied to absorption due only to phytoplankton (data not shown, but see Bricaud et al., 1995, 1998); note that the two lines are almost parallel. (b) Spectral absorption coefficients (log scale) for pure water, a_w (Pope and Fry, 1997), and as modeled for natural seawater with three chlorophyll concentrations. Note that the red absorption peak (675 nm) of chlorophyll (Fig. 2) is totally overwhelmed by water absorption. Therefore, this absorption capability of phytoplanktonic algae is irrelevant, in as much as there is no available red light in marine environments.

$$b_p(550) = 0.416\ [Chl]^{0.766} \qquad (5)$$

Based on other measurements and theoretical considerations, the spectral coefficient, $b_p(\lambda)$, is usually given a wavelength dependency according to λ^{-1} (Mie-type scattering).

The second step consists of adopting a value for the backscattering probability (i.e., of the ratio b_{bp}/b_p). In the absence of direct determinations, the resort to theoretical considerations is currently necessary, together with the inverted use of Eq. 2 (when both R and a have been measured, and f computed via the RTE). This ratio varies between about 1.5% in clear waters and 0.4% in Chl-rich waters. Clearly, some uncertainties still remain for this important parameter and, therefore, limit the capability of the semi-analytical approach.

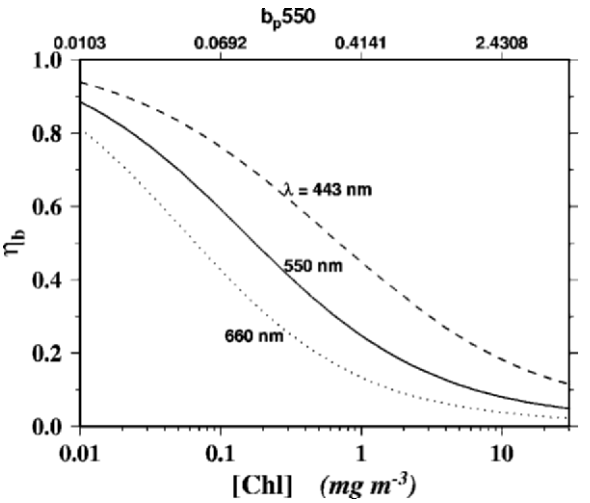

Fig. 5. Ratio $\eta_b = b_{bw} / (b_{bw}+b_{bp})$ of the backscattering by water molecules (Morel, 1974) to the total backscattering coefficient (molecules + particles), as a function of the chlorophyll concentration (log-scale), and at the three wavelengths as indicated.

IV. Reflectance of Oceanic Waters

With the parameterizations summarized above, and by using Eq. 2, a full spectral model for reflectance can be built (Fig. 6a). It accounts well for the spectral reflectance determined in the field (Fig. 6b). The ratio of two reflectances at two wavelengths, already shown in Fig. 3, is derived from this model, and is an example of a semi-analytical algorithm. When [Chl] increases, the reflectance in the blue part of the spectrum strongly decreases and a minimum develops around 430 nm (as a result of pigment absorption); meanwhile, the green reflectance increases (as a result of the increase in b_b), so that a maximum develops around 565 nm. In the red part of the spectrum (beyond 600 nm), R is always low (<0.2% in oligotrophic waters and <1% in eutrophic waters) whereas a relative maximum centered at 683 nm appears. This Gaussian peak (half height bandwidth ≅ 20 nm) corresponds to the sun-stimulated fluorescence emission of phytoplankton, which adds to the backscattered flux (Morel and Prieur, 1977; Gordon, 1979). This emission is separately modeled by computing the incident solar (400–660 nm) photons captured by algae by using $a_\varphi(\lambda)$, and by assuming a fluorescence quantum yield of 0.8% which is typical of cells inhabiting the well-lit oceanic upper layers (Maritorena et al., 2000; see also their Eq. 7 for the computation of the fluorescence emission). In this spectral domain, Raman scattering by water molecules, excited by shorter wavelengths, is not negligible. It may contribute about 10% to the reflectance observed beyond 600 nm in clear waters, and less when [Chl] increases. This emission has been measured, either directly (Sugihara et al., 1984; see also Fig. 6b), or via the Fraunhofer line filling method (see Hu and Voss, 1997), and can be accurately modeled.

V. Phytoplankton Distribution and Primary Production

Once the spectral radiances emerging from the water have been extracted from the total signal recorded above the atmosphere (see Section VII), blue-to-green ratios are calculated; then, with these ratios and by use of algorithms (i.e., the polynomial fit to curves as shown in Fig. 3), [Chl] is retrieved for each pixel in the scene. The [Chl] distribution in the world's oceans can thus be obtained (examples shown in Fig. 7). Such algorithms are valid only for oceanic Case 1 waters. When applied to complex Case 2 coastal waters (about 3% of the world ocean), such algorithms generally fail and lead to large overestimates of [Chl]. Consequently, locally-adapted algorithms, which are still being developed, are necessary for such coastal waters (IOCCG, 2000).

As the marine radiances originate only from the upper layer of the ocean, the exact significance of the retrieved [Chl] deserves examination. It has been shown (Gordon and McCluney, 1975) that 90% of the emerging photons originate from a layer having a thickness equal to the 'penetration depth' (the depth where the downward radiation is reduced to 1/e (i.e., 37%) of its initial value beneath the surface. This depth varies with [Chl], from about 20 m in clear oligotrophic waters to a few meters in eutrophic waters. Therefore, the estimated [Chl] can be considered as a weighed average of the chlorophyll concentration within this upper layer. Since phytoplankton can live and grow at a depth, known as the euphotic depth, where the PAR (photosynthetically active radiation) is reduced to only 1% (or even 0.1%) of its subsurface value, only a fraction (about one fifth) of the productive algal biomass is 'seen' by a remote sensor. This physical limitation is similar to that faced with terrestrial vegetation: the optical signal originates mainly from the canopy. This is an inescapable limitation when trying to assess the potential primary production of the entire biomass. Fortunately, however, rather robust statistical relationships exist between

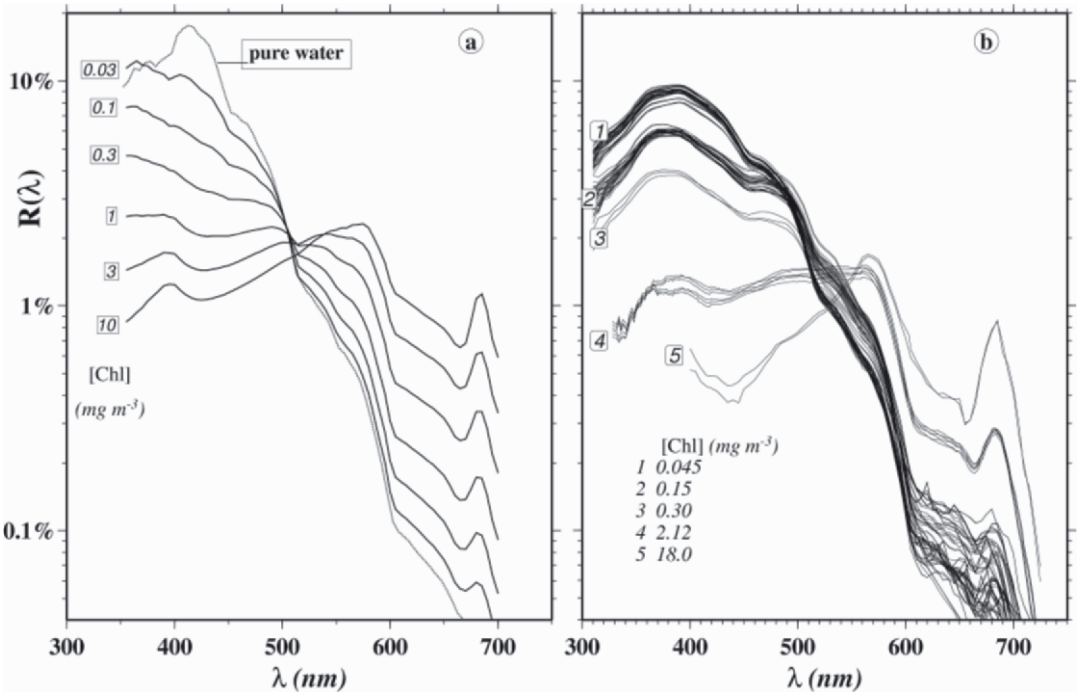

Fig. 6. (a) Reflectance spectra produced by a semi-analytical model (see text and Morel and Maritorena, 2001) for various chlorophyll concentrations. Note that these spectra account for Raman scattering and Chl *a* fluorescence (peak around 685 nm). The hypothetical reflectance spectrum computed for pure seawater is also shown. (b) Selected examples of reflectance spectra (Eq. 1), as determined at sea, in various locations with differing chlorophyll concentrations. Curves 1, 2, and 3 from the central Pacific, 4 from the Moroccan upwelling zone, and 5 from the Mauritanian upwelling zone.

the near-surface [Chl] and the vertical chlorophyll profile (Morel and Berthon, 1989); thus, in practice, this difficulty can be circumvented. The stability of the water column (depicted by the vertical profile of water density) is also involved in shaping the chlorophyll profile.

In essence, the prediction of the column integrated primary production is based on a triple integration (with respect to wavelength, time, and depth) of the instantaneous and local net photosynthesis equation (Morel, 1991). This equation involves the photo-physiological parameters derived from the production-irradiance curve (the so-called P-vs-E, curve), and a temperature dependency for the maximal, light-independent, production (the so-called P^{max} quantity). This equation is spectrally dependent through the algal absorption spectrum, $a^*(\lambda)$, combined with the spectral distribution of available light at any depth which is considered. When dealing with the global ocean and satellite information, the input parameters for the model are firstly, the day and latitude, which govern the day length together with the time course of photosynthetically available radiation (PAR) availability at the surface (computed via an atmospheric model) by assuming that the sky is clear; secondly, the cloudiness index, also derived from satellite data, which modulates PAR, and; thirdly, the sea surface temperature (SST), which is also detected from space. Knowing [Chl] in the surface layer (and the associated vertical chlorophyll profile), the computation consists of propagating PAR (and its spectral composition) throughout the water column, down to the euphotic depth, and then of entering the photosynthesis equation with the local [Chl]. Fortunately, these complex calculations can be made in advance for all possible cases thus providing lookup tables for practical use in conjunction with the time, date and latitude together with SST, cloudiness, and [Chl] information obtained from the satellite (Antoine and Morel, 1996). Various simplifications of the above scheme are also in use (e.g., Platt, 1986; Behrenfeld and Falkowski, 1997b). Parameterizing the photo-physiological response of algae remains a difficult and sensitive issue in comparison with the physical aspects of the problem,

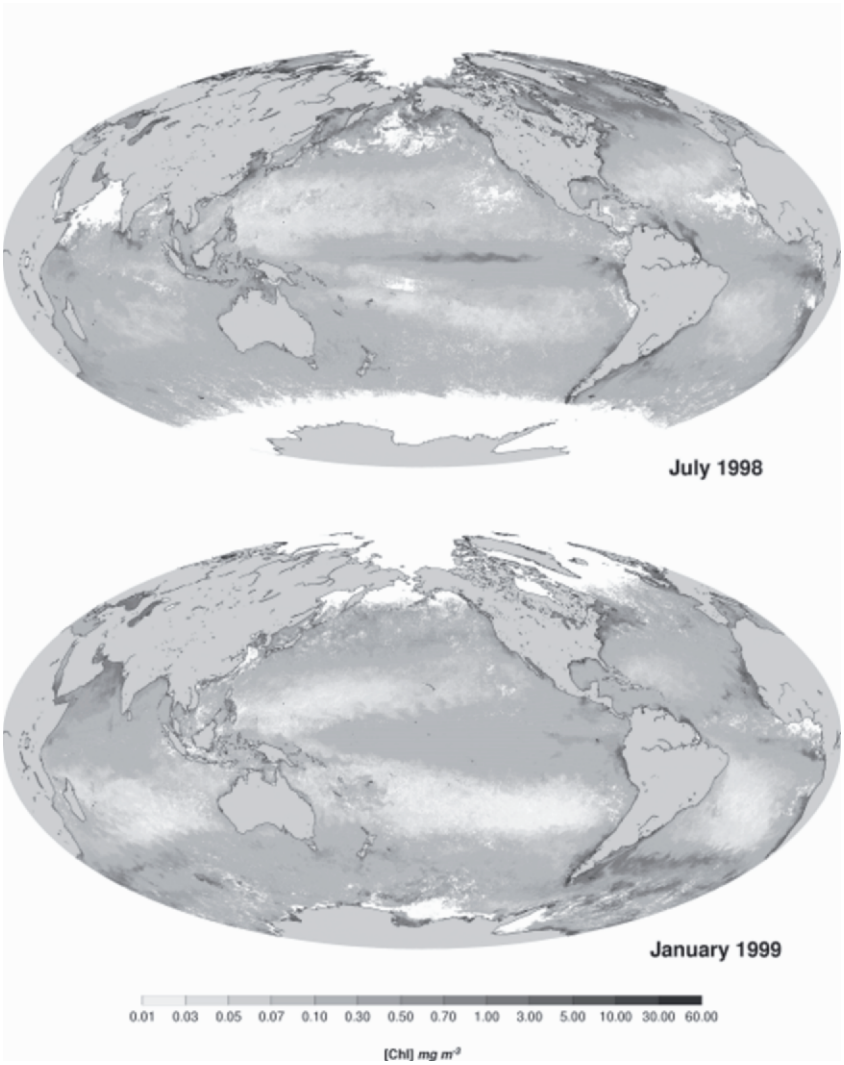

Fig. 7. Examples of global maps of chlorophyll concentration (color encoding indicated) within the oceanic upper layer, as derived from observations by the SeaWiFS sensor. Similar maps are produced on a daily basis; they are, however, incomplete, because of coverage limitations and presence of clouds. By merging daily maps, weekly, monthly, and yearly averages can be produced. Shown here are monthly averaged maps for two opposite seasons, July 1998 and January 1999. Even over one month, some areas remain unseen (clouds masked in white). The high latitude zones, alternatively in the Northern (January) or Southern (July) hemispheres, which are either ice covered,or too dark and in the polar night, are also masked in white. These maps show the permanence and extension of the oligotrophic deep blue subtropical gyres, and in-between, of the equatorial divergence which sustains an enhanced algal biomass. Spring-early summer blooms occur alternatively in both hemispheres at latitudes beyond 40°. The upwelling systems, induced by the trade winds, support high biomasses along the coasts of South Africa, Angola, Mauritania, Senegal, Chile, Peru. In the northeast Indian ocean sector, probably one of the most productive zones of the ocean, the situation is more complex because of the alternation of opposite monsoons in summer and winter. See also Color Plate 8.

which are more easily and safely modeled.

Global annual photosynthetic carbon fixation (called NPP, net primary production), as derived from previous space observation (CZCS), were converging around a value of 50 Pg C per year (Petagram = Pg = 10^{15}g) (Longhurst et al., 1995, Antoine et al., 1996, Behrenfeld and Falkowski, 1997a). Interestingly, with such a value, now confirmed by new estimates based on SeaWiFS imagery, the annual carbon fixation through marine photosynthesis appears to be similar to that realized by terrestrial vegetation (Field et al., 1998). Therefore, the average turnover time of the oceanic biomass is much shorter than for the terrestrial biomass (1 week vs. about 15 years),

because of their disproportionate sizes in terms of carbon biomasses (1 vs 700 Pg C approximately for the marine and terrestrial vegetation, respectively). Such a disproportion is obviously in keeping with the typical generation cycle time (i.e., years for terrestrial plants, and hours for unicellular algae). Geographic and seasonal variations in oceanic primary production can now be studied with an unprecedented amount of detail thanks to ocean color imagery: even if the absolute estimates of NPP become more accurate in the future, the errors currently incurred are probably small.

VI. Sun-stimulated Fluorescence

Algal biomass has been estimated at sea for more than 30 years using chlorophyll fluorescence, by means of active excitation techniques (Lorenzen, 1966). Passive (sun-induced) fluorescence has also been detected in reflectance spectra (Morel and Prieur, 1977). The use of this signal as a possible remote sensing technique for phytoplankton determination has been suggested (Neville and Gower, 1977) and sensors, such as MODIS and MERIS, now provide adequate spectral channels (Table 1). One narrow channel is centered on the red emission peak (683 nm), and two others, on each side of the peak, help to define a baseline permitting the fluorescence intensity to be quantified. In contrast to the conventional color ratio technique, fluorescence provides a specific signal, as it originates only from Chl *a* within the antenna of Photosystem II. This signal emitted in a narrow spectral band is added to the reflectance spectrum, and its amplitude is essentially unaffected by the presence of other optically active substances (at least when the turbidity is not too high). Therefore, a method based on its detection seems particularly useful in complex coastal Case 2 waters, where the color ratio technique generally fails. Further, there is no obstacle in extending it to Case 1 waters, at least when [Chl] exceeds 0.4 $mg \bullet m^{-3}$ (as occurs in about 10–20% of the world's oceans), which makes Chl fluorescence radiometrically detectable from space (Babin et al., 1996; Gower et al., 1999). There is, however, a serious disadvantage due to the strong water absorption in this spectral domain: the red signal which emerges, emanates only from the very upper water layer (about 1–2 m thick) thus only providing information about the near-surface [Chl].

The interpretation of fluorescence in terms of phytoplanktonic biomass is difficult. Indeed, the signal (the fluorescence line height) depends not only on [Chl] itself, but also on the intensity of the excitation, and on the realized fluorescence quantum yield, ϕ_f. Therefore, normalizing the fluorescence signal by the incident flux could provide an estimate of the biomass only if both the absorption capability of algae per unit of Chl *a* and ϕ_f were either invariant or easily derivable from other observable quantities. The absorption capability factor is known to be variable (Fig. 4b) and ϕ_f, the second factor, can also vary at least 5-fold depending on species, physiological state and radiation availability which rule the photochemical and non-photochemical quenching processes (Falkowski and Kiefer, 1985, Kiefer and Reynolds, 1992). Unfortunately, at a local level, the slopes of linear relationships between the fluorescence signal and [Chl] have been found to change widely with time and location (Gower et al., 1999). On the spatial and temporal scales involved in space observation, the possibility of reliably predicting ϕ_f, which would permit the fluorescence image to be readily transformed into quantitative chlorophyll maps, is still questioned. However, the comparison of fluorescence emission with the biomass, as derived through the conventional band ratio technique, could provide important information about the physiological state and photosynthetic performances of the algal crop. The relationship between fluorescence and photosynthesis, however, is not straightforward (Westberry and Siegel, 2003; Falkowski et al., 2004; Moya and Cerovic, 2004). Presently, the issue of non-photochemical quenching of fluorescence (an important source of variability) remains an obstacle in the comprehensive and systematic application of these fluorescence techniques.

VII. Concluding Remarks: The Atmospheric Correction

A reader, having learned in the first paragraph that the marine signal, to be interpreted in terms of chlorophyll concentration, represents a very small fraction of the signal captured by a satellite-borne sensor, will be curious to know how this problem is solved. This process is euphemistically called 'the atmospheric correction,' because the corrective term largely exceeds the desired variable (Gordon and Morel, 1983). For the sake of completeness, a brief overview of this corrective scheme follows.

For each spectral channel, the total radiance (λ omitted) recorded by a satellite-borne sensor at the top of the atmosphere, L_T (W m^{-2} $sr^{-1}\mu m^{-1}$), can be written in a simplified way as (see also Fig. 1)

$$L_T = L_R + L_A + L_{RA} + (L_F + L_G) + t^* L_W \quad (6)$$

To get the marine information, namely, $t^* \bullet L_W$, which represents the radiance leaving the water (L_W) modified by the atmospheric diffuse transmittance factor ($t^* < 1$), all other terms have to be estimated and then subtracted from L_T. The first three terms correspond to radiances generated by atmospheric scattering and reflection (sky reflection) at the interface (the paths 1, 1', 2, and 2', in Fig. 1); the subscripts R, A, and RA indicate the nature of the scattering events, which may occur only with air molecules (R for Rayleigh), or suspended aerosols (A), or both successively, via multiple scattering (the coupling term L_{RA}). These atmospheric terms depend on the geometry; namely, on the viewing angle and the zenith-sun angle, and involve the molecular (Rayleigh) and aerosol (Mie) scattering phase functions. They must be assessed by solving numerically the RTE, with the appropriate atmospheric input parameters. The two other terms to be subtracted are related to the local wind speed; namely, the additional radiance L_F, which is generated by the foam forming the white caps, and L_G (or 'glitter') which represents the sun radiation reflected by capillary waves, outside of the specular image itself (called the 'sun glint'). The knowledge of the wind field, associated with geometrical considerations, allows these terms to be estimated.

The above decomposition of the signal actually demonstrates that, besides [Chl], other unknowns appear in the ocean color remote sensing problem. The crucial additional unknown is the aerosol load (and nature), which governs the magnitude and the spectral behavior of the terms L_A and L_{RA}. Other unknowns, besides the wind speed, are the barometric pressure which reflects the number of air molecules and thus directly modulates Rayleigh scattering and the vertically integrated ozone content (an absorbing gas which influences t*). Ancillary data, derived from other satellite sensors or meteorological records, are used for estimating these three parameters and the corresponding corrections.

Regarding aerosols, however, there is no independent information that can be used. Therefore, an autonomous and co-located (i.e., pixel-by-pixel) solution must be found, based on the data provided by the sensor itself. In essence, the solution consists of using two well-founded assumptions: firstly, the Rayleigh scattering term can be computed with any desired accuracy at all wavelengths and, secondly, in the near infra-red (NIR), the ocean is black ($L_W = 0$), at least for Case 1 waters. Therefore, L_A and L_{RA} can be retrieved at two wavelengths in the NIR (see Table 1), assuming L_F and L_G can be constrained. The magnitude of L_A and L_{RA} is an indicator of the aerosol load (i.e., its optical thickness). The spectral dependency of these terms, as observed between the two wavelengths, is used for the identification of the nature of the aerosol and then for the extrapolation of aerosol scattering toward the visible part of the spectrum. These extrapolated values are subtracted to derive $t^* L_W$ in the visible part of the spectrum; then t* is computed, based on the aerosol optical thickness, and finally the quantities L_W can be retrieved. Such a correction scheme implies an extensive manipulation of the RTE for all possible geometrical configurations and for all possible aerosol 'models' (which differ by their phase functions and spectral behaviors). Pre-computed lookup tables are needed to speed up the processing of such data.

In spite of its complexity, this procedure has proven to be very efficient in most situations, but natural and computational limitations exist. Obviously, when the aerosol optical thickness becomes too high, the ocean signal vanishes, as also occurs in the presence of clouds. Some absorbing aerosols, such as soot from forest fires or industrial wastes or desert dust spreading over the ocean, are difficult to deal with. Also, the initial hypothesis of 'black' pixel in the NIR may fail, and often does, in coastal turbid areas, indicating that other techniques need to be employed. Interestingly, when the correction process works it provides extremely valuable information, as a by-product, about the aerosol distribution over the open ocean, which remains a crucial component of the radiation budget of our planet.

Acknowledgments

I thank H. Claustre, P. Falkowski, B. Genty, M. Lewis, J. Ras, and A. Sciandra for critically reading this manuscript, B. Gentili for the preparation of the figures, and the NASA Goddard-DAAC for providing the SeaWiFS data.

References

Antoine D and Morel A (1996) Oceanic primary production. 1. Adaptation of a spectral light-photosynthesis model in view of application to satellite chlorophyll observations. Global Biogeochem Cycles 10: 43–55

Antoine D, André J-M and Morel A (1996) Oceanic primary production. 2. Estimation at global scale from satellite (coastal zone color scanner) chlorophyll. Global Biogeochem Cycles 10: 56–69

Babin M, Morel A and Gentili B (1996) Remote sensing of sea surface sun-induced chlorophyll fluorescence; consequences of natural variations in the optical characteristics of phytoplankton and the quantum yield of chlorophyll *a* fluorescence. Int J Remote Sensing 17: 2417–2448

Behrenfeld MJ and Falkowski PG (1997a) Photosynthetic rates derived from satellite-based chlorophyll concentration. Limnol Oceanogr 42: 1–20

Behrenfeld MJ and Falkowski PG (1997b) A consumer's guide to phytoplankton primary productivity models. Limnol Oceanogr 42: 1479–1491

Bricaud A, Babin M, Morel A and Claustre H (1995) Variability in the chlorophyll-specific absorption coefficients of natural phytoplankton: Analysis and parameterization. J Geophys Res 100: 13321–13332

Bricaud A, Morel A, Babin M, Allali K and Claustre H (1998) Variations of light absorption by suspended particles with chlorophyll a concentration in oceanic (Case 1) waters: Analysis and implications for bio-optical models. J Geophys Res 103: 31033–31044

Bricaud A, Claustre H, Ras J, and Oubelkheir K (2004) Natural variability of phytoplanktonic absorption in oceanic waters: Influence of the size structure of algal populations. J Geophys Res 109: C11010,doi:10.1029/2004JC002419, 2004

Clarke GL and Ewing GC (1974) Remote spectroscopy of the sea for biological production studies. In: Jerlov NG and Steeman-Nielsen E (eds) Optical Aspects of Oceanography, pp 389–413. Academic Press, New York

Duysens LM (1956) The flattening of the absorption spectra of suspensions as compared to that of solutions. Biochim Biophys Acta 19: 1–12

Falkowski PG and Kiefer DA (1985) Chlorophyll *a* fluorescence in phytoplankton, relationship to photosynthesis and biomass. J Plankton Res 7: 715–731

Falkowski PG, Koblizek M, Gorbunov M and Kolber M (2004) Development of variable fluorescence techniques in marine ecosystems. In: Papageorgiou GC and Govindjee (eds) Chlorophyll *a* Fluorescence: A Signature of Photosynthesis, pp 757–778. Springer, Dordrecht

Field C, Behrenfeld M, Randerson J and Falkowski P (1998) Primary production of the biosphere: Integrating terrestrial and oceanic components. Science, 281: 237–240

Gordon HR (1979) Diffuse reflectance of the ocean: The theory of its augmentation by chlorophyll-*a* fluorescence at 685 nm. Appl Opt 18: 1161–1166

Gordon HR and McCluney WR (1975) Estimation of the depth of sun light penetration in the sea for remote sensing. Appl Opt 14: 413–416

Gordon HR and Morel A (1983) Remote Assessment of Ocean Color for Interpretation of Satellite Visible Imagery: A Review. Springer Verlag, New York

Gower JFR, Doerffer R and Borstad GA (1999) Interpretation of the 685 nm peak in water-leaving radiance spectra in terms of fluorescence, absorption and scattering, and its observation by MERIS. Int J Remote Sensing 20:1771–1786

Hu C and Voss KJ (1997) In situ measurements of Raman scattering in clear ocean water. Appl Opt 36: 6962–6966

IOCCG (International Ocean Color coordinating Group) (1998) Minimum Requirements for an Operational Ocean-Color Sensor for the Open Ocean. In: Morel A (ed) IOCCG Report No. 1, pp 46. Dartmouth NS, Canada

IOCCG (International Ocean Color Co-ordinating Group) (2000) Remote Sensing of Ocean Colour in Coastal, and Other Optically-Complex, Waters. In: Sathyendranath S (ed) IOCCG Report No. 3, pp 140. Dartmouth NS, Canada

Kiefer DA and Reynolds RA (1992) Advances in understanding phytoplankton fluorescence and photosynthesis. In: Falkowski PG and Woodhead AD (eds) Primary Productivity and Biogeochemical Cycles in the Sea, 155–174. Plenum Press New York and London

Kishino M, Takahashi M, Okami N and Ichimura (1985) Estimation of the spectral absorption coefficients of phytoplankton in the sea. Bull Mar Sci 37: 634–642

Lee Z, Carder KL, Hawes SK, Steward RG, Peacock TG and Davis CO (1994) Model for the interpretation of hyperspectral remote-sensing reflectance. Appl Opt 33: 5721–5732

Loisel H and Morel A (1998) Light scattering and chlorophyll concentration in case 1 waters: A reexamination. Limnol Oceanogr 43: 847–858

Longhurst A, Sathyendranath S, Platt T and Caverhill C (1995) An estimate of global primary production in the ocean from satellite radiometer data. J Plankton Res 17: 1245–1271

Lorenzen CJ (1966) A method for the continuous measurement of in vivo chlorophyll concentration. Deep-Sea Res 13:223–227

Maritorena S, Morel A and Gentili B (2000) Determination of the fluorescence quantum yield by oceanic phytoplankton in their natural habitat. Appl Opt 36: 6725–6737

Morel A (1974) Optical properties of pure water and pure sea water. In: Jerlov NG and Steeman-Nielsen E (eds) Optical Aspects of Oceanography, pp 1–24. Academic Press, New York

Morel A (1991) Light and photosynthesis: A spectral model with geochemical and climatological implications. Prog Oceanogr 26: 263–306

Morel A and Berthon J-F (1989) Surface pigments, algal biomass profiles, and potential production of the euphotic layer: Relationships reinvestigated in view of remote sensing applications. Limnol Oceanogr 34: 1545–1562

Morel A and Bricaud A (1981) Theoretical results concerning light absorption in a discrete medium, and application to specific absorption of phytoplankton. Deep-Sea Res 28, 1375–1393

Morel A and Maritorena S (2001) Bio-optical properties of oceanic waters: A reappraisal. J Geophys Res 106: 7163–7180

Morel A and Prieur L (1977) Analysis of variations in ocean color. Limnol Oceanogr 22: 709–722

Moya I and Cerovic ZG (2004) Remote sensing of chlorophyyll fluorescence: Instrumentation and analysis. In: Papageorgiou GC and Govindjee (eds) Chlorophyll *a* Fluorescence: A Signature of Photosynthesis, pp 429–445. Springer, Dordrecht

Neville RA and Gower JFR (1977) Passive remote sensing of phytoplankton via chlorophyll *a* fluorescence. J Geophys Res 82: 3487–3493

O'Reilly JE, Maritorena S, Mitchell BG, Siegel DA, Carder KL, Garver SA, Kahru M and McClain C (1998) Ocean color chlorophyll algorithms for SeaWiFS. J Geophys Res 103: 24937–24953

Platt T (1986) Primary production of the ocean water column as a function of surface light intensity: Algorithms for remote sensing. Deep Sea Res 33:149–163

Pope RM and Fry ES (1997) Absorption spectrum (380–700 nm) of pure water, II, Integrating cavity measurements. Appl Opt 36: 8710–8723

Smith RC and Baker KS (1978) The bio-optical state of ocean waters and remote sensing. Limnol Oceanogr 23: 247–259

Stramski D, Bricaud A and Morel A (2001) Modeling the inherent optical properties of the ocean based on the detailed composition of the planktonic community. Appl Opt 40: 2929–2945

Sugihara S, Kishino M and Okami N (1984) Contribution of Raman scattering to upward irradiance in the sea. J Oceanogr Soc Jap 40: 397–404

Westberry T K, and Siegel D A (2003) Phytoplankton natural fluorescence variability in the Sargasso Sea. Deep-Sea Res I, 50: 417–434

Yentsch CS (1962) Measurement of visible light absorption by particulate matter in the ocean. Limnol Oceanogr 7:207–217